GEM NEWS INTERNATIONAL

Contributing Editors
Gagan Choudhary, *IIGJ-Research & Laboratories Centre, Jaipur, India* (gagan.choudhary@iigjrlc.org)
Christopher M. Breeding, *GIA, Carlsbad* (christopher.breeding@gia.edu)
Guanghai Shi, *School of Gemmology, China University of Geosciences, Beijing* (shigh@cugb.edu.cn)

COLORED STONES AND ORGANIC MATERIALS

The special color effect in "chameleon" amber. One special variety of Burmese amber is "chameleon" amber, named for the bluish green color that appears to float on its surface (figure 1). This material is found in the famous Tengchong market in Yunnan Province, China's largest Burmese amber market. Its bodycolor ranges from golden brown to brownish red or even red (figure 2A). When exposed to sunlight or strong white light against a black background, its surface shows a uniform green color (figure 2B). Chameleon amber is rare and expensive compared to regular Burmese golden or brownish amber, especially with the severe reduction of exports from Myanmar.

Until recently, few studies have been conducted on chameleon amber. X. Jiang et al. speculated that the green surface color might be caused by the superposition of its bodycolor and the fluorescence of amber ("Gemmological and spectroscopic characteristics of different varieties of amber from the Hukawng Valley, Myanmar," *Journal of Gemmology*, Vol. 37, No. 2, 2020, pp. 144–162). C.C. Shuai et al. proposed that the "light retention" effect was related to elevated sulfur and calcium contents ("The spectrum characteristic research of color change effect and 'light tarry effect' amber from Burma," *Spectroscopy and Spectral Analysis*, Vol. 40, 2020, pp. 1174–1178). Z. Shi et al. reported that the effect might be due to unique internal aromatic hydrocarbon structures ("Spectral characteristics of unique species of Burmese amber," *Minerals*, Vol. 13, No. 2, 2023, article no. 151).

Editors' note: Interested contributors should send information and illustrations to Stuart Overlin at soverlin@gia.edu.

Gems & Gemology, Vol. 59, No. 3, pp. 388–412.

For this study, three Burmese chameleon amber specimens were acquired from the Tengchong market (see figures 1, 2A, and 3A). All three displayed a translucent brownish red bodycolor, with a few bubbles and flow lines within them. The bluish green floating color was observed when the specimens were rotated. This phenomenon is most obvious with a black background. Standard gemological properties and Fourier-transform infrared spectroscopy data were consistent with those of regular Burmese amber. While the bluish green floating color might be related to fluorescence, no such effect is seen on other types of fluorescing Burmese amber (e.g., brownish amber). To further explore this, brownish Burmese amber beads with bodycolor similar to that of chameleon amber were selected as a reference (figures 2C and 3C). Their bodycolor was not as vivid as chameleon amber, and it did not display the bluish green floating fluorescence. Observation under a UV lamp showed

Figure 1. A good-quality 88.25 ct "chameleon" amber with a red bodycolor displaying a vivid green fluorescence color that appears to float on the surface. Photo by Yan Li.

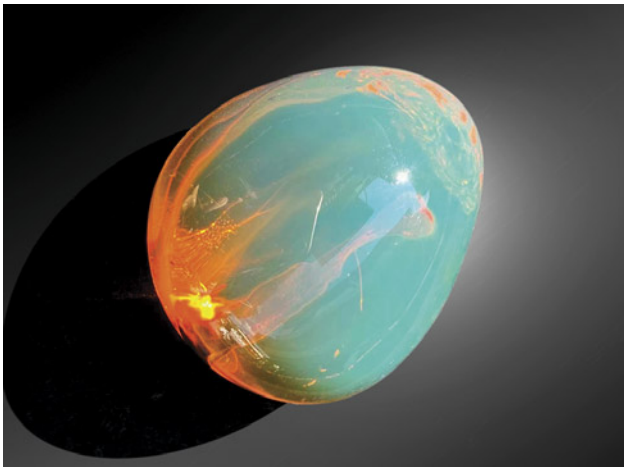

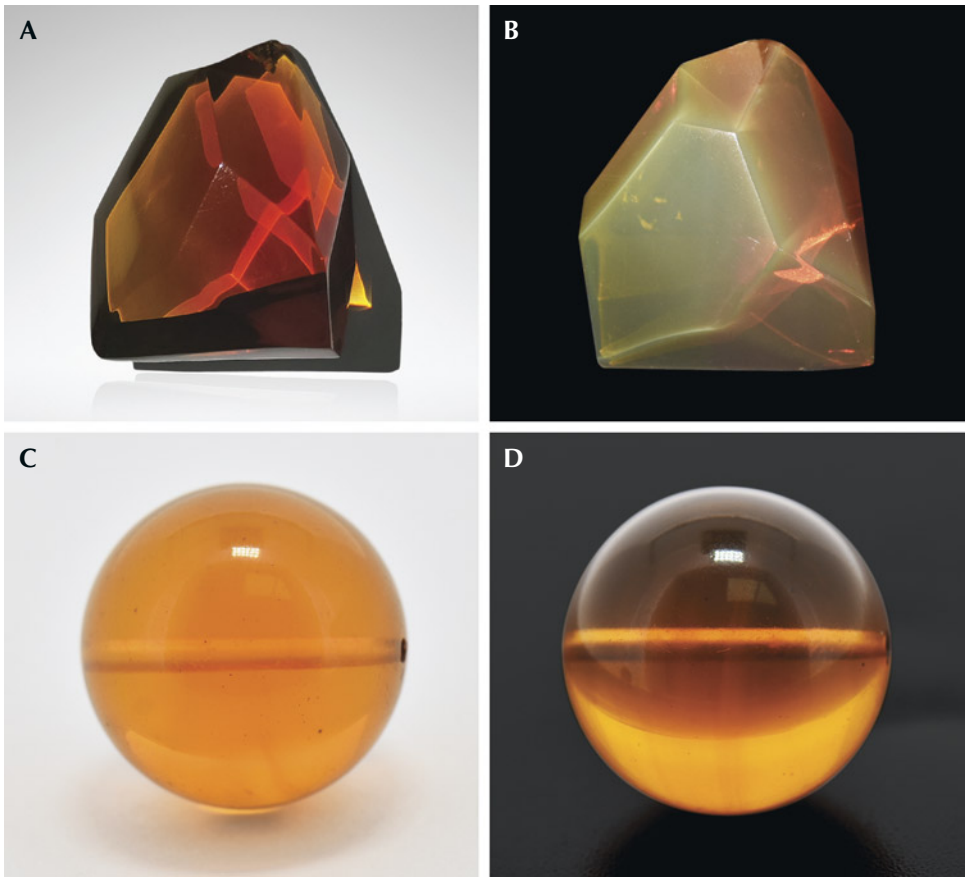

Figure 2. A and B: A 78.51 ct chameleon amber exposed to white light against white and black backgrounds. C and D: A 12.50 ct brownish reference sample exposed to similar lighting and backgrounds. Photos by Jinfeng Yang.

that the chameleon amber in figure 3A produced strong bluish white fluorescence (figure 3B) in long-wave UV (365 nm), while the brownish amber beads in figure 3C showed a weak bluish purple fluorescence (figure 3D).

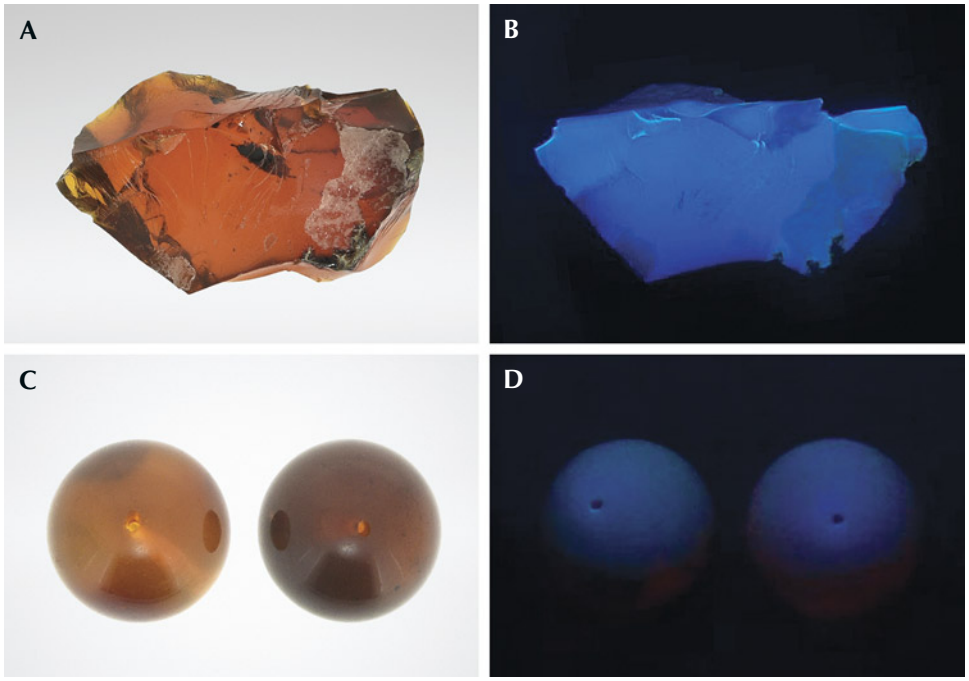

Figure 3. A and B: A 71.05 ct Burmese chameleon amber and its bluish white fluorescence under long-wave UV light. C and D: 16 mm brownish Burmese amber beads (12.60 ct on the left, 12.16 ct on the right) and their bluish purple fluorescence under long-wave UV. Photos by Jinfeng Yang.

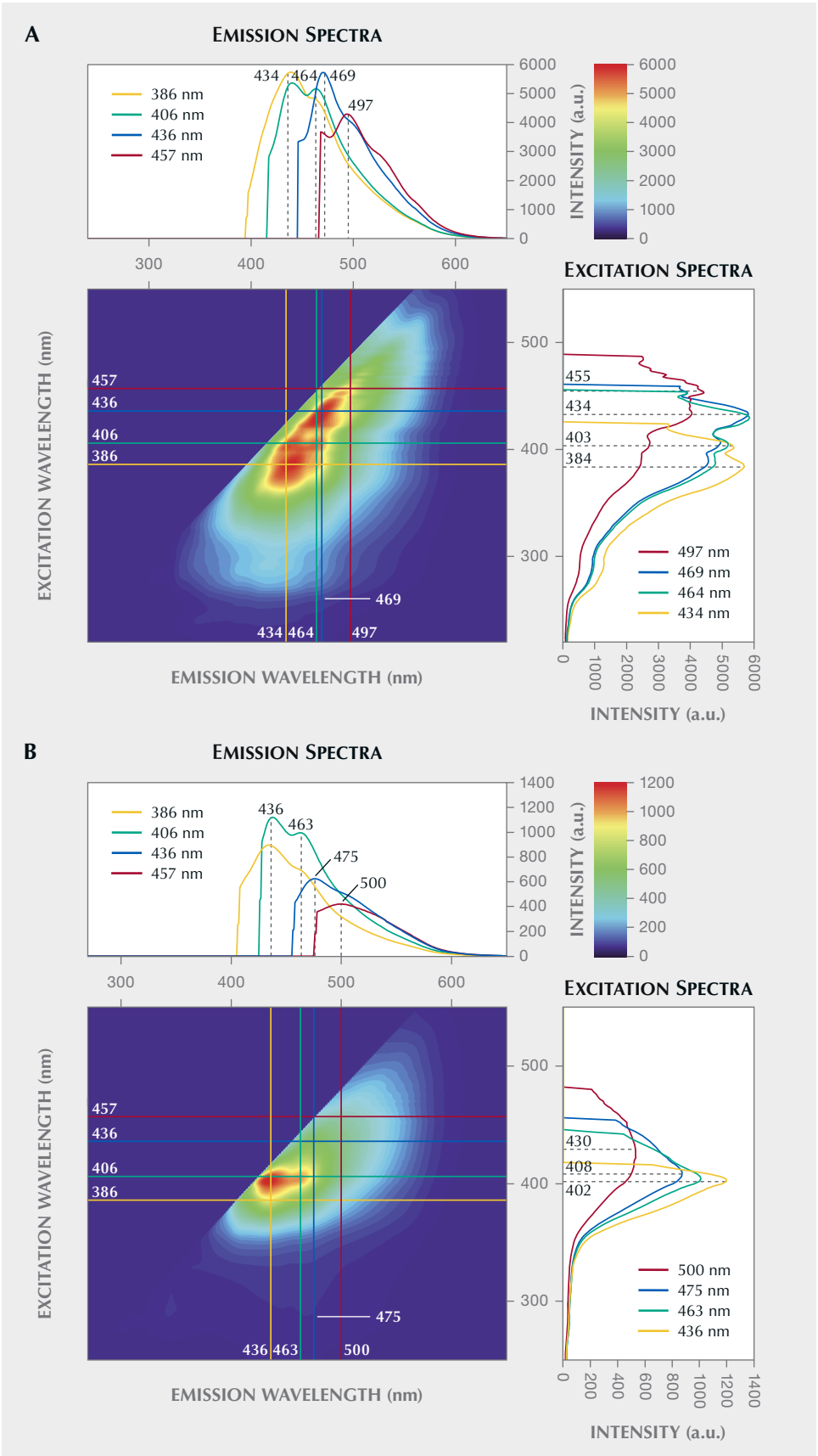

Figure 4. 3D fluorescence spectra of Burmese chameleon amber (A) and brownish amber (B).

The samples were then examined with 3D fluorescence spectroscopy (figure 4) under the excitation of a continuous-wavelength excitation light source. The fluorescence intensity of brownish amber was clearly much lower than that of chameleon amber. In addition, two peaks (455 and 384 nm) were absent in the excitation spectrum of brownish amber. A high degree of similarity was exhibited in the samples' emission spectra, with all the peaks positioned at approximately 434, 464, 469, and 497 nm. However, the biggest difference was in the fluorescence intensity, which was easily observed in chameleon amber.

The 3D fluorescence spectra of chameleon amber exhibited several fluorescence centers, mainly at 434, 464, 469, and 497 nm generated by excitation wavelengths of 386, 406, 436, and 457 nm. The fluorescence color could be calculated by the fluorescence centers, and the results showed that the spectral color was blue under 386 nm excitation and bluish green under 436 nm excitation. We believe that the bluish green floating color under sunlight is caused by the bluish green fluorescence center at 469 nm under 436 nm excitation. This is much more consistent with observations in daylight. Due to the low fluorescence intensity of brownish amber, its blue fluorescence color is very weak, and most light penetrates it without producing any special optical effect. The difference in fluorescence intensity between the 469 and 434 nm fluorescence centers corresponds with the relative spectral power distribution of the light source. Under the excitation of a xenon lamp, the fluorescence center at 434 nm is more intense than the light-emitting center at 469 nm. However, amber is usually observed in daylight. The optimal excitation wavelengths for the emission centers at 434 and 469 nm are 386 nm and 436 nm, respectively. From the relative spectral power distribution of the two light sources, it can be seen that the spectral density of the xenon lamp at 386 nm is greater than 436 nm, while the D65 daylight-equivalent source is the opposite. Against a dark background and under daylight, the fluorescence of chameleon amber should be dominated by the bluish green fluorescence emitted at 436 nm.

The fluorescence center at 469 nm is very common in Baltic, Dominican, Mexican, and Burmese amber. This fluorescence center in chameleon amber is unique for its high intensity and separation from other fluorescence colors. Only if the fluorescence intensity is high enough will it show as the dominant fluorescence color. The optimal excitation wavelength (436 nm) corresponding to the 469 nm fluorescence center is far removed from the optimal excitation wavelength of other strong fluorescence centers; therefore, the fluorescence color is not a mixture of multiple colors. Many varieties of amber can also produce strong fluorescence at 469 nm, but often mixed with other fluorescence colors of similar intensity. For example, the fluorescence peaks of 448 and 474 nm in Dominican blue amber always appear together, and their strong fluorescence peaks can be seen with exposure to the same excitation wavelength. In most cases, the fluorescence intensity of the former is slightly greater, which leads to the fluorescence of the blue amber being mainly blue, without a green modifier. Some Dominican blue amber with uneven fluorescence distribution can also show a mosaic pattern (X. Chenxing et al., "Characterisation of patchy blue and green colouration in Dominican blue amber," *Journal of Gemmology*, Vol. 37, No. 7, 2021, pp. 700–713). The fluorescence distribution of the chameleon amber tested in this study was uniform, with high intensity and good separation, producing a high-quality bluish green floating fluorescence effect.

Jinfeng Yang, Yan Li, and Youzhi Liang
Gemmological Institute
China University of Geosciences, Wuhan

A newly discovered iridescent andradite from Inner Mongolia, China. Iridescent garnet found in Chifeng City, Inner Mongolia, was recently encountered in the Chinese market. Iridescent garnet was first discovered in 1943 in the U.S. state of Nevada (E. Ingeron and J.D. Barksdale, "Iridescent garnet from the Adelaide Mining District, Nevada," *American Mineralogist*, Vol. 28, 1943, pp. 303–312), and it is also found in Mexico and Japan (M.A. Badar and M. Akizuki, "Iridescent andradite garnet from the Sierra Madre Mountains, Sonora, Mexico," *Neues Jahrbuch für Mineralogie - Monatshefte*, Vol. 1997, No. 12, pp. 529–539; T. Hainschwang and F. Notari, "The cause of iridescence in rainbow andradite from Nara, Japan," Winter 2006 *G&G*, pp. 248–258). To the authors' knowledge, this is the first report of iridescent garnet in China. Two rough samples were collected by the authors in the Lindong lead mining area (figure 5). The refractive index was over the limits of a conventional refractometer, and the hydrostatic specific gravity values were 3.85 and 3.84. Both showed an inert reaction to long- and short-wave ultraviolet fluorescence. These standard gemological testing results were consistent with garnet.

On the basis of energy-dispersive X-ray fluorescence, calcium, silicon, iron, aluminum, manganese, magnesium, titanium, and sodium were detected. The chemical composition of the larger sample was analyzed using electron probe microanalysis (EPMA). The composition was consistent with that of andradite, containing major elements of calcium, iron, aluminum, and silicon, with the derived chemical formula of $(Ca_{3.015}Mn_{0.031}Na_{0.006}Mg_{0.003}Ti_{0.002})(Fe_{1.846}Al_{0.138})[Si_{2.978}O_{12}]$. The backscattered electron image showed clear growth layers (figure 6, left). Aluminum in the darker zones was about 2 wt.% higher on average than in the lighter zones, and the iron content decreased with increasing aluminum. Raman spectroscopic analysis involved comparison with the RRUFF database (B. Lafuente et al., https://rruff.info/about/downloads/HMC1-30.pdf). The peak positions (figure 7) indicated that the samples were consistent with those of andradite, supporting the composition inferred from EPMA. Raman shifts within 300 to 400 cm^{-1} were assigned to SiO_4 rotational vibrations. Raman shifts within 400 to 700 cm^{-1} were caused by Si-O_{bend} (bridge oxy-

Figure 5. Iridescent andradite samples (25 ct and 125 ct) from the Lindong area of Inner Mongolia, China. As shown in the left photo, sample G-1 displays iridescence on the (211) plane but not on the (110) plane. Photos by Jiuchang Yang.

gen) bending and asymmetric stretching vibrations. Raman shifts at 800 to 1200 cm^{-1} were attributed to the characteristic absorption peak of Si-O_{str} stretching vibration (B.A. Kolesov and C.A. Geiger, "Raman spectra of silicate garnets," *Physics and Chemistry of Minerals*, Vol. 25, No. 2, 1998, pp. 142–151).

Figure 6. Left: Growth layers viewed normal to the (110) crystal face in a backscattered electron (BSE) image from a polished thin section. Right: The iron and aluminum contents corresponding to each spot in the BSE image.

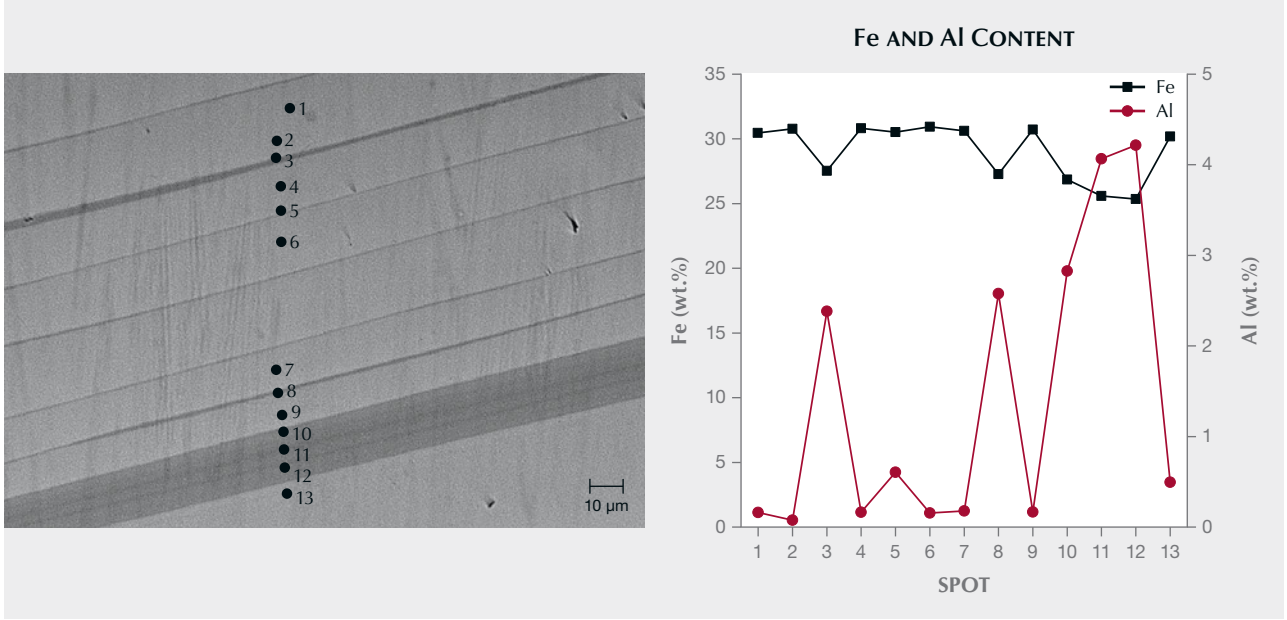

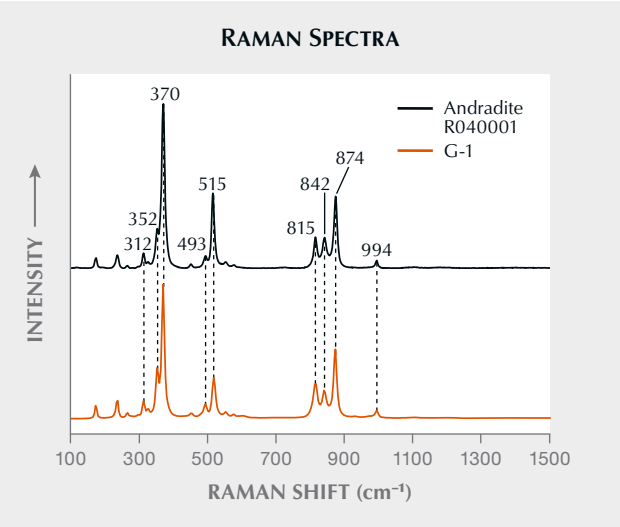

Figure 7. Sample G-1 was identified as andradite based on a comparison with a sample from the RRUFF database. Spectra are offset vertically for clarity.

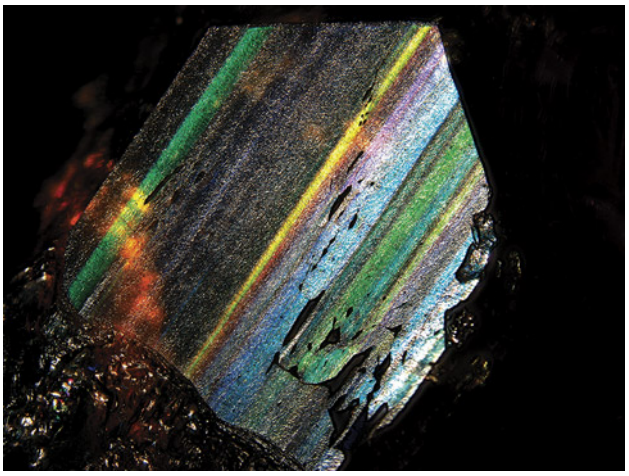

Figure 8. Sample G-1 displays strong iridescence with a full spectrum of colors. For certain bands, the color does not change as the viewing angle changes. This image is of a face parallel to (211). Photomicrograph by Jiuchang Yang; field of view 24.45 mm.

Microscopic observation revealed an attractive play-of-color with a complete visible spectrum of colors on the (211) crystal plane of sample G-1 (figure 8). We cut three polished thin sections from sample G-2 along the (110) and (211) crystallographic axes to observe the twinning structure and extinction phenomena under a polarizing microscope. The sample displayed angled layered growth structures and a strong grid-like pattern and abnormal birefringence (figure 9). A grid-like extinction phenomenon parallel to the growth layer (figure 9A) may have been caused by lattice-like twins, and figure 9C shows two areas with different extinction orientations. One study on Japanese andradite showed that the iridescence effect is caused by the alternate growth of iron-rich layers and aluminum-rich layers. These layers cause a thin-film interference phenomenon in the crystal struc-

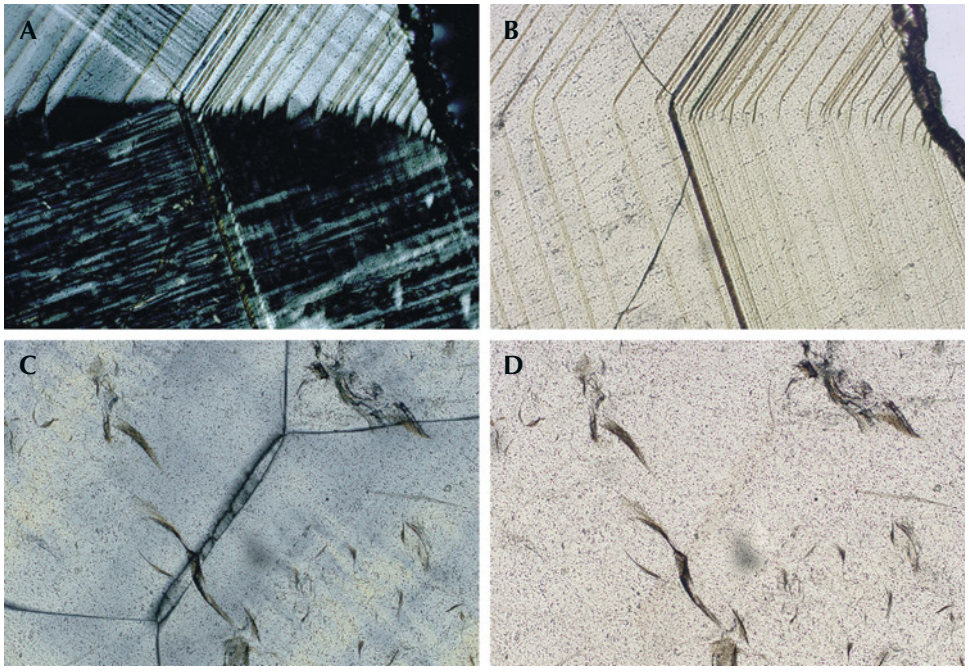

Figure 9. Top: The polished thin section in A and B was cut normal to the (110) crystal face. Observation under crossed polarizers (A) showed strong grid-like pattern, abnormal birefringence (possibly caused by lattice-like twinning), and angled growth bands. Bottom: The section in C and D was cut parallel to the (110) crystal face. Observation under crossed polarizers (C) showed partitioned abnormal birefringence caused by contact twinning and faint growth bands. Photomicrographs by Jiuchang Yang; field of view 25.05 mm.

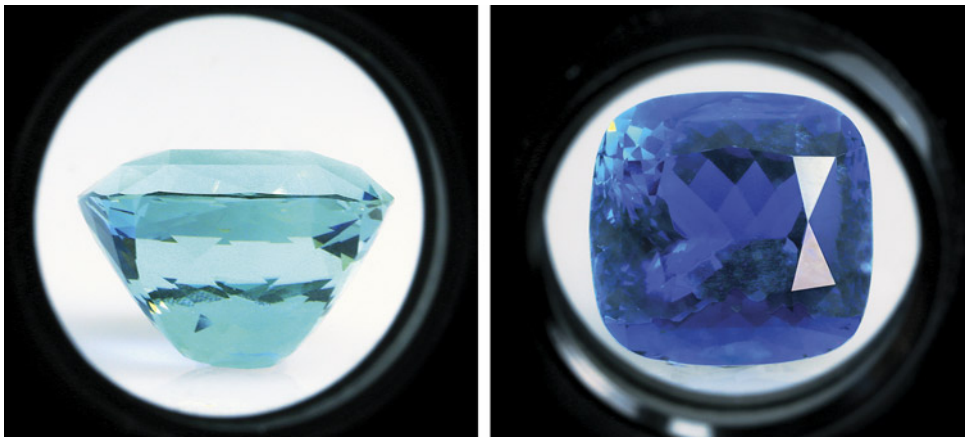

Figure 10. A 55 ct cushion-cut aquamarine exhibiting a distinct light bluish green and deep blue pleochroism using a dichroscope. Photos by Kaiyin Deng; courtesy of Farrugia Gem.

ture (Hainschwang and Notari, 2006). Therefore, we speculate that the iridescence of andradite from the Lindong lead mining area is not closely related to twinning but may be closely related to thin-film interference caused by its layered growth structure.

Jiuchang Yang, Quanli Chen (chenquanli@cug.edu.cn), Fengshun Xu, and Yan Li
Gemmological Institute
China University of Geosciences, Wuhan

Xianyu Liu
College of Jewelry, Shanghai Jian Qiao University

Aquamarine with zigzag growth line inclusions. A 55 ct cushion-cut aquamarine (figure 10, left) was recently submitted to Guild Gem Laboratories in Shenzhen for testing. This stone exhibited a very intense blue color accompanied by a subtle greenish secondary hue. A refractive index of 1.580–1.586 was obtained, together with a specific gravity of approximately of 2.71. Fourier-transform infrared (FTIR) and Raman spectroscopy confirmed its identity as beryl. The transmission FTIR spectrum exhibited distinct peaks at 2731, 2686, and 2641 cm^{-1} and a carbon dioxide–related signal at 2359 cm^{-1}. Peaks at 3235, 3162, 3111, and 3021 cm^{-1} were assigned to the presence of water (figure 11, left). This collection of FTIR peaks has been reported in natural aquamarine, but no synthetic counterpart has been reported to show this pattern (I. Adamo et al., "Aquamarine, Maxixe-type beryl, and hydrothermal synthetic blue beryl: Analysis and identification," Fall 2008 *G&G*, pp. 214–226). No organic-related peaks were found around the 2800–3200 cm^{-1} range, suggesting no clarity enhancement had been applied (L. Jianjun et al., "Polymer-filled aquamarine," Fall 2009 *G&G*, pp. 197–199). Strong deep blue and light bluish green pleochroism (figure 10) was observed using a dichroscope. Similar beryl materials with a deep blue color have been reported in previous studies (Fall 2014 GNI, pp. 244–245; Fall 2019 GNI, pp. 437–439). The ultraviolet/visible/near-infrared spectrum (figure 11, right) showed a broad Fe^{2+}-related band centered at around 835 nm and narrow absorption bands at 370 and 426 nm related to Fe^{3+} (D.S. Goldman et al., "Channel constituents in beryl," *Physics and Chemistry*

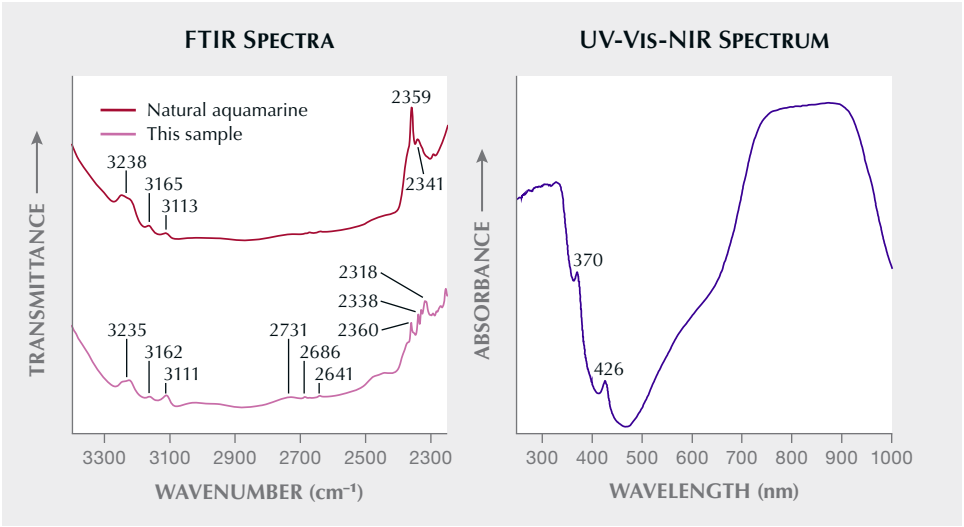

Figure 11. Infrared transmission spectra (left) and UV-Vis-NIR spectrum (right) of the aquamarine sample. The spectra on the left are offset vertically for clarity.

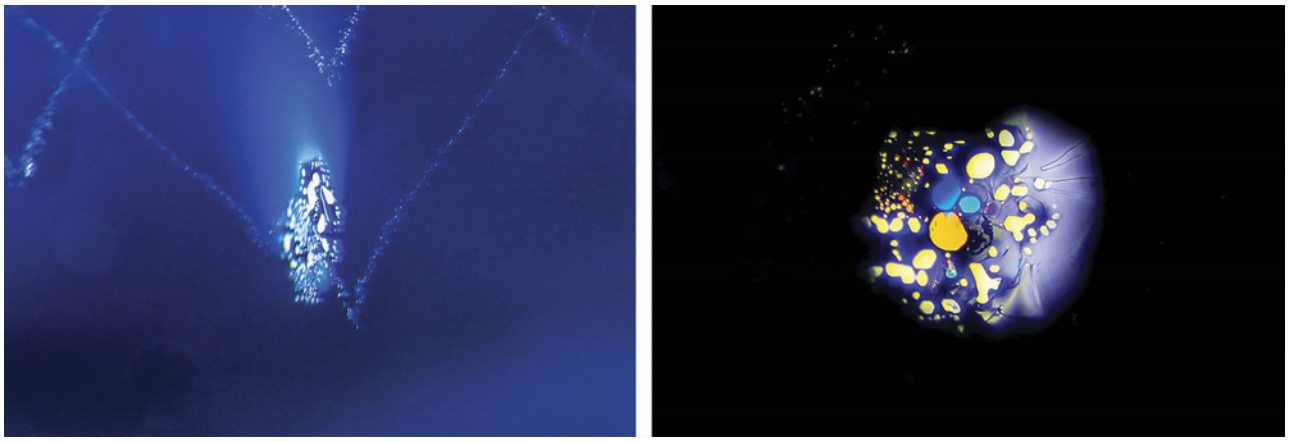

Figure 12. The thin film along the basal plane of the aquamarine under fiber-optic illumination. Photomicrographs by Yizhi Zhao; fields of view 3.45 mm (left) and 1.72 mm (right).

of Minerals, Vol. 3, No. 3, 1978, pp. 225–235; K. Schmetzer, "Hydrothermally grown synthetic aquamarine manufactured in Novosibirsk, USSR," Fall 1990 *G&G*, pp. 206–211; Adamo et al., 2008). Using a polariscope equipped with a conoscope, the optic axis was observed parallel to the table along the long axis of the cushion shape. Further chemical analysis by energy-dispersive X-ray fluorescence showed a high iron content (around 13000 ppmw), which likely contributed to the saturated blue color (Y. Shang et al., "Spectroscopy and chromaticity characterization of yellow to light-blue iron-containing beryl," *Scientific Reports*, Vol. 12, No. 1, 2022, article no. 10765).

Microscopic observation under darkfield illumination revealed fluid inclusions and minute voids. Under the table, a circular thin film with a strong light reflection was visible (figure 12). The image in figure 12 (left) was captured at an angle to the table of the aquamarine, since the thin film was easier to see under an oblique light source. Because beryl has imperfect cleavage along its basal plane {0001}, the space between the basal planes caused by initial cleavage was sufficient to form the thin film.

An interesting inclusion was observed only with oblique light: a distinct series of fluids resembling dots and broken lines. Higher magnification (figure 13) revealed that these zigzag lines consisted of discrete and minute fluid inclusions. Further observation along the optic axis confirmed that the planes were parallel to the *c*-axis of the aquamarine.

A previous study described similar inclusions in emeralds from Colombia as resembling a DNA double helix (Summer 2019 *G&G* Micro-World, p. 262). The authors have also encountered this type of inclusion before. Based on our observations, these helical inclusions spiral along the optic axis of the emerald. To our knowledge, this is the first time such helical inclusions have been reported in an aquamarine. This finding will help advance our understanding of the beryl family.

Yujie Gao, Xueying Sun (shirley.sun@guildgemlab.com), Yizhi Zhao, and Kaiyin Deng
Guild Gem Laboratories
Shenzhen, China

Figure 13. Zigzag lines were observed in the aquamarine using oblique light. Photomicrograph by Yizhi Zhao; field of view 4.52 mm.

Blackish green omphacite jade from Guatemala. In recent years, a new kind of Guatemalan jade has entered the Chinese jewelry market, where it is called *yongchuliao fei cui* (or *yongchuliao* for short). Prior to the availability of yongchuliao, Chinese consumers had a negative impression of Guatemalan material and preferred Burmese jade. However, the recent emergence of this new high-quality blackish green jade has attracted the attention of Chinese buyers.

The authors recently tested a rough stone and a carved pendant of yongchuliao (figure 14). Under reflected light, these samples appeared blackish green with a greasy luster similar to Burmese inky black jade. The rough stone was opaque and had numerous fine white inclusions measuring approximately 300 μm in diameter on its surface. The

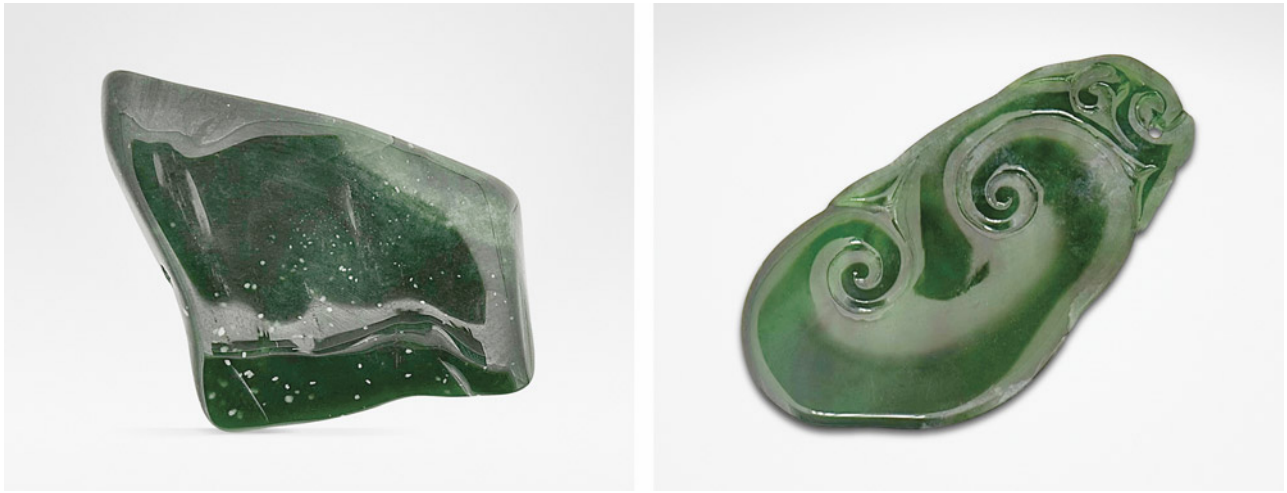

Figure 14. Yongchuliao *samples collected for testing. The rough sample on the left weighs 30.1 ct, and the carving on the right weighs 12.85 ct. Photos by Shilong Xu.*

carved sample was bright green with coarse texture and medium transparency under transmitted light (figure 15). The rough and carved samples had a refractive index of 1.67 and specific gravities of 3.342 and 3.332, respectively. These gemological characteristics are consistent with both jadeite-type jade and omphacite-type jade.

Qualitative analysis using energy-dispersive X-ray fluorescence spectrometry revealed magnesium, aluminum, silicon, calcium, chromium, manganese, and iron, among other elements. It should be noted that the ideal chemical formula of jadeite is $NaAlSi_2O_6$ and that of omphacite is $(Ca,Na)(Mg,Fe,Al)Si_2O_6$ (S.F. McClure, "The jadeite/omphacite nomenclature question," *GIA Research News*, April 12, 2012). Jadeite and omphacite can form a complete solid solution. The occurrence of calcium, magnesium, and other elements implies that the mineral composition of yongchuliao is not pure jadeite.

Raman shifts at 681, 514, 411, 378, 340, and 209 cm^{-1} were consistent with those of omphacite (figure 16). The Raman spectra of fibrous inclusions in the carved sample also matched those of omphacite rather than jadeite. The strongest Raman shift at 681 cm^{-1} was attributed to the symmetrical Si-O-Si stretching vibration (B. Xing et al., "Locality determination of inky black omphacite jades from Myanmar and Guatemala by nondestructive analysis," *Journal of Raman Spectroscopy*, Vol. 53, No. 11, 2022, pp. 2009–2018). Raman spectroscopy was used to compare the samples' mineral composition against the RRUFF database (B. Lafuente et al., https://rruff.info/about/downloads/HMC1-30.pdf), revealing that yongchuliao material

Figure 15. Left: Fibrous inclusions observed in the 12.85 ct carved sample; field of view 8.94 mm. Right: The carved sample appeared bright green rather than blackish green under transmitted light. Photos by Shilong Xu.

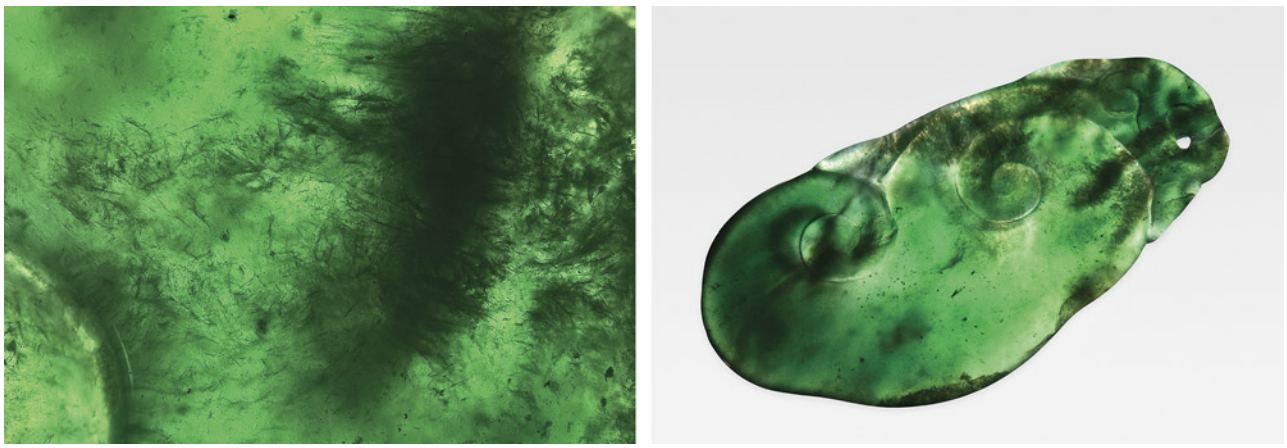

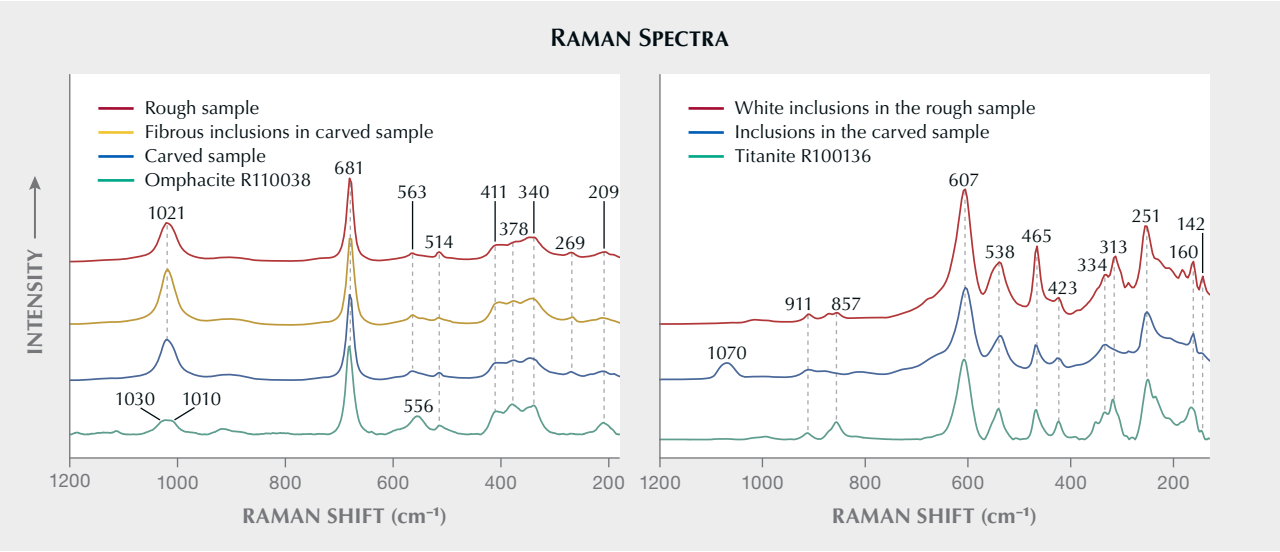

Figure 16. The mineral species were confirmed by comparison with samples from the RRUFF database. Spectra are offset vertically for clarity. Left: The host mineral and fibrous inclusions of the samples matched with omphacite. Right: The white dotted mineral inclusions in the rough sample matched with titanite. Titanite in the carved sample could also be observed in micro-Raman imaging.

consists almost entirely of omphacite. The fine white inclusions distributed evenly in the rough sample were coincident with titanite (figure 16). In addition, some of the sample was ground into powder for X-ray diffraction analysis to obtain the mineral composition of the whole rock. The results showed an omphacite content of about 98.49% (with a 5% margin of error), and the rest was magnesian calcite. The results from Fourier-transform infrared absorption spectroscopy were consistent with the Raman spectra, identifying the main mineral composition of the samples as omphacite.

A double-sided polished piece was cut from the rough sample for testing. Its ultraviolet/visible/near-infrared (UV-Vis-NIR) absorption spectrum (figure 17) showed an absorption peak at 437 nm, indicating the presence of Fe^{3+}. Absorption peaks at 637, 657, and 688 nm were also observed and attributed to Cr^{3+} (G.R. Rossman, "Color in gems: The new technologies," Summer 1981 *G&G*, pp. 61–62).

Based on testing, both samples were omphacite-type jade containing titanite inclusions. Since almost all of the yongchuliao we have observed exhibited nearly the same colors and textures as these samples, it is likely that other yongchuliao may also have similar mineral compositions.

Figure 17. In the UV-Vis-NIR spectrum of a piece cut from the rough sample, absorption peaks were observed within the visible range at 437, 637, 657, and 688 nm.

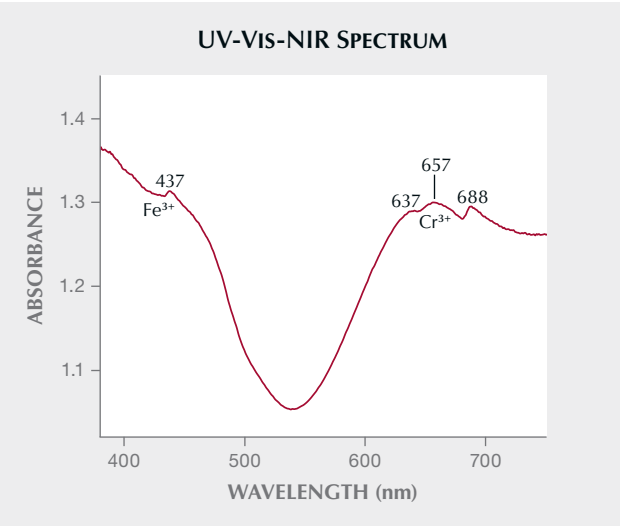

Shilong Xu, Quanli Chen (chenquanli@cug.edu.cn), and Yan Li
Gemmological Institute
China University of Geosciences, Wuhan

Xianyu Liu
College of Jewelry, Shanghai Jian Qiao University

Shell blister on an *Isognomon isognomon* shell. Theoretically, all mollusks are capable of producing pearls, but only a small number of them actually produce commercially traded nacreous pearls. Most come from the *Pinctada* and *Pteria* genera belonging to the *Pteridae* family. Species that produce the nacreous pearls regularly seen in the market, such as *Pinctada maxima*, *Pinctada radiata*, *Pteria sterna*, and *Pteria penguin*, are well known to aficionados. However, some unusual bivalve species can also produce pearls or shell blisters, and one example was recently submitted to GIA's Mumbai laboratory for scientific examination.

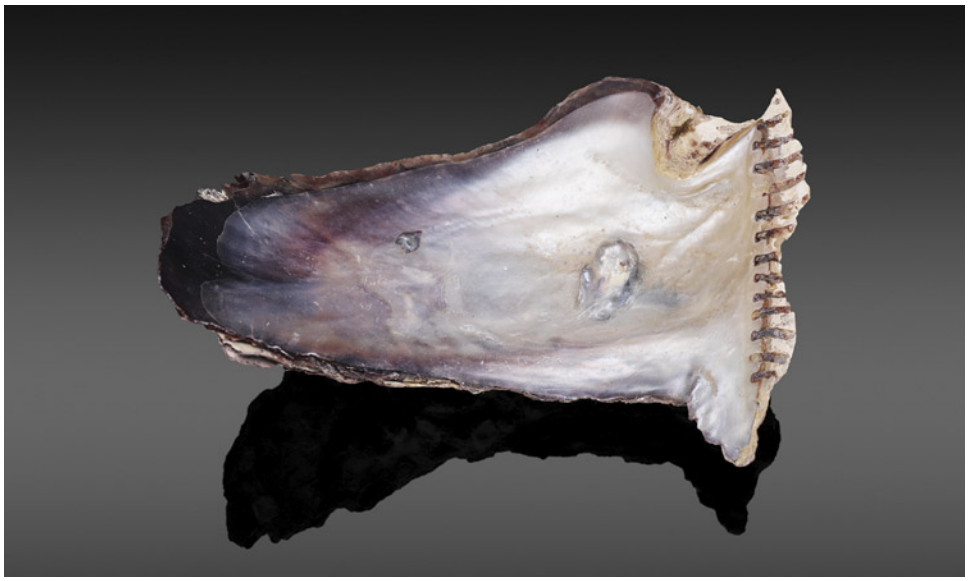

Figure 18. Isognomon isognomon *shell and blister. The shell measures approximately 107.76 × 72.39 mm. Photo by Gaurav Bera.*

The shell was from the *Isognomon isognomon* species, belonging to the *Isognomonidae* family and commonly known as the Pacific toothed oyster. It exhibited a blister feature that appeared as a folded section of nacre, located near the center, close to the posterior muscle scar and the hinge (figure 18). The shell weighed 46.88 g and measured approximately 107.76 × 72.39 mm, while the baroque-shaped silver to light gray blister measured approximately 8.80 × 4.21 mm. Not all instances of nacre growth on a shell are classified as pearls. While cyst pearls or whole pearls develop independently from the shell, blisters are nacreous concretions that appear to protrude from the shell (K. Lawanwong et al., "Natural shell blisters and blister pearls: What's the difference?" *GIA Research News*, August 26, 2019). According to the pearl classification established by CIBJO, the concretion observed on the shell in question would be categorized as a shell blister.

The shell itself displayed a narrow, elongated shape, featuring a straight hinge with distinct equidistant dark brown notches along its length (figure 19, left). These notches, also known as resilifers or ligament pits, resemble teeth, giving the species its common name; see I. Temkin and C. Printrakoon, "Morphology and taxonomy of *Isognomon spathulatus* (Reeve, 1858), a cryptic bivalve from the mangroves of Thailand," *Zootaxa*, Vol. 4107, No. 2, 2016, pp. 141–174.

The interior of the shell exhibited a predominantly nacreous aragonite surface, characterized by a discernible spiral platelet structure visible under microscopic exami-

Figure 19. Left: Dark brown rows of notch-like features observed on the hinge of the shell. Right: A whitish subsurface dendritic network of parasite channels. Photomicrographs by Prasad Mane; fields of view 16.3 mm (left) and 6.1 mm (right).

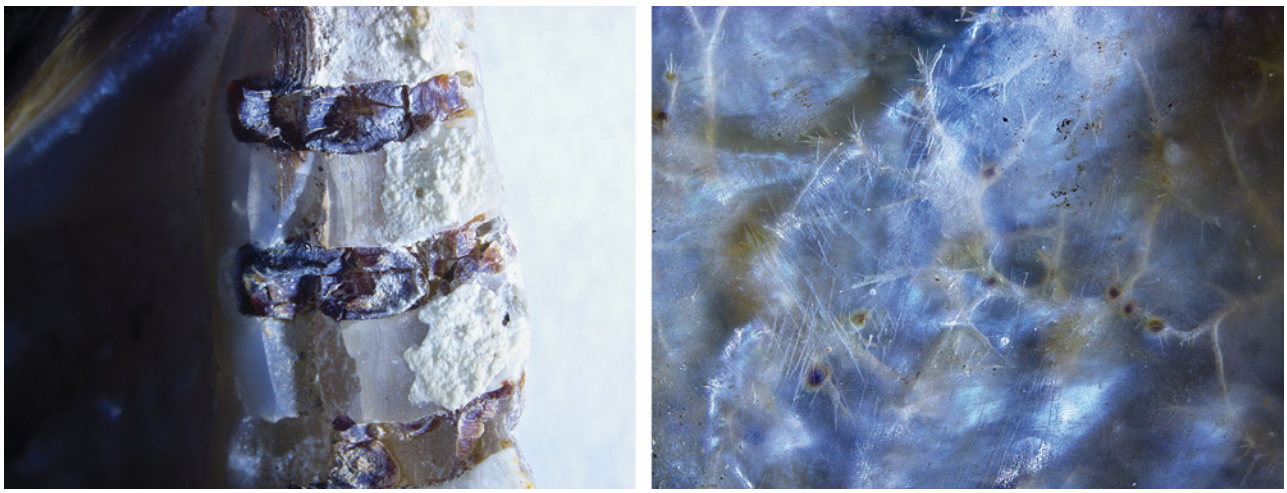

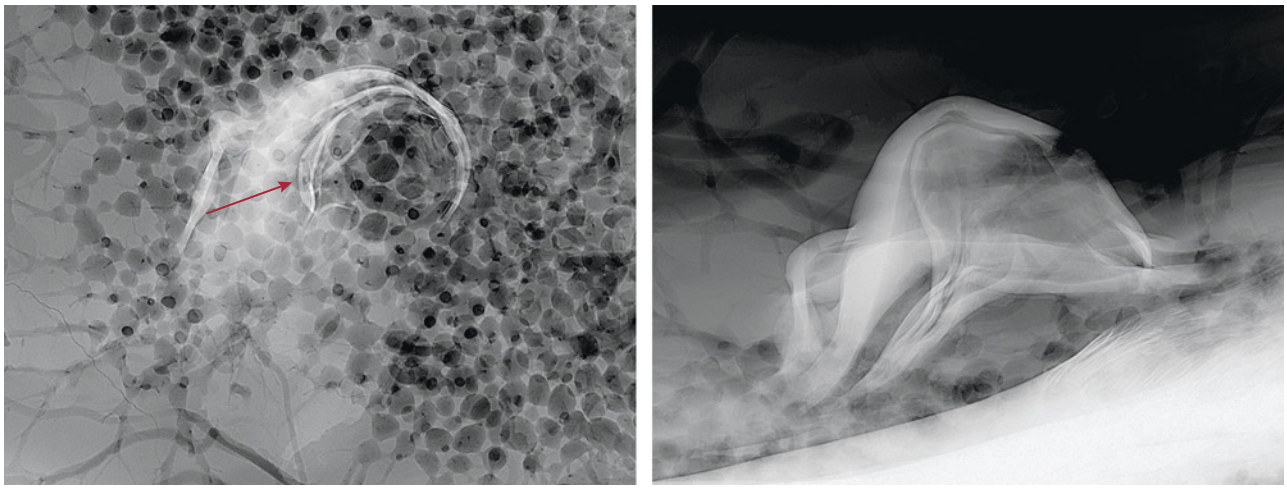

Figure 20. Left: RTX image of the top view of the 8.80 × 4.21 mm shell blister (arrow) with a network of parasitic boreholes and channels visible around it. Right: RTX image of the side of the shell blister with more radiopaque folds marking its outline.

nation. This nacreous region was bordered by a non-nacreous shell margin. The central nacre displayed a light gray coloration, transitioning to a darker purplish gray toward the margin. The center of the shell had a more translucent appearance, revealing a subsurface dendritic network of parasitic channels surrounding the blister (figure 19, right).

Real-time microradiography (RTX) revealed a network of fine channels beneath the blister and throughout the shell itself (figure 20, left). These features corresponded to the parasitic channels observed within the translucent layer on the shell's interior. RTX imaging of the blister revealed a void (figure 20, right), potentially linked to parasitic activity that may have initiated the blister formation.

X-ray fluorescence (XRF) imaging of both the shell and the blister yielded an inert reaction. Energy-dispersive X-ray fluorescence spectrometry of the blister indicated a manganese level below the instrument's detection limit and a strontium level of 1135 ppm. The inert XRF reaction, along with the chemical composition, proved the mollusk formed in a saltwater environment. Under long-wave UV radiation, the shell displayed a greenish yellow fluorescence reaction, while short-wave UV radiation yielded an inert response. Raman analysis using a 514 nm ion/argon laser excitation revealed peaks at 701/704 cm^{-1} and 1085 cm^{-1}, indicative of aragonite. Photoluminescence spectra collected from both the shell and the blister showed three broad peaks centered at 620, 650, and 680 nm, which is observed in some naturally colored pearls.

Although the *Isognomonidae* family and the *Pteridae* family belong to the Pteroidae superfamily, pearls from oysters such as the Pacific toothed oyster (*Isognomon isognomon*) are rarely seen. Therefore, it was intriguing to examine this blister. Perhaps we will someday encounter a natural pearl from this mollusk species.

Prasad Mane, Nishka Vaz, and Abeer Al-Alawi
GIA, Mumbai

Mining basalt-related gems in southeast Vietnam. A number of gemstone deposits are known in provinces all across Vietnam. These include ruby (Yen Bai and Nghe An), sapphire (Yen Bai, Nghe An, Binh Thuan, and Dak Nong), spinel (Yen Bai and the Central Highlands), aquamarine (Thanh Hoa and Khanh Hoa), tourmaline and garnet (Yen Bai), and peridot (Gia Lai). Recently, seven gemstone occurrences have been identified within the basaltic fields in southeast Vietnam, which are mainly found in Dong Nai and Ba Ria–Vung Tau provinces. These gems include sapphire, zircon, garnet, augite, brown peridot, feldspar, and hyalite opal. They are found predominantly in basalt bedrock and its regolith as xenocrysts or xenoliths deposited on hillslopes or in placer formations along streambeds. Seven gemstone species from southeast Vietnam were collected and documented (figure 21).

The sapphires usually appeared as hexagonal crystals or fragments, exhibiting mainly blue, deep to dark greenish blue, and greenish yellow colors. Most were transparent to semitranslucent and some opaque, and the luster was greasy to vitreous. The typical rough sizes ranged from 5 to 20 mm, weighing 2–10 ct.

Euhedral tetragonal crystals of zircon were very common, while the rest of them were fragmented. Colors included orange, brown-red, gray, and colorless. These zircon samples showed high luster ranging from adamantine to vitreous, with a transparent to semitransparent appearance. Zircons from southeast Vietnam were not found in fresh basalt; they were found mostly in placer and in weathered basalt instead (figure 22A).

"Red stone" is a local name for gem-quality garnet from Dong Nai. The garnets occurred in two forms of anhedral fragments: xenocrystic fragments (also called "orphan stone") weighing 1–50 ct, with a corroded surface, and xenolith-hosted garnet containing small corroded fragments that produce 1–5 ct fashioned gems. Both xenocryst (figure 22B)

Figure 21. Gem materials from southeast Vietnam. The three largest yellow and white samples on the far left are feldspar, while the brown, orange, and near-colorless samples in the center are zircon and the two greenish white samples near the top right are hyalite opal. The rest of the dark stones are sapphires, garnets, augites, and brown peridot. Photo by Le Ngoc Nang; courtesy of Tran Ngoc Vien.

and xenolith-hosted garnet were found mainly in the regolith on the hillslopes. The color ranged from deep to dark red and occasionally deep orangy yellow, with a transparent to semitransparent quality and a vitreous luster.

Euhedral crystals of Dong Nai feldspar were characterized by two directions of perfect cleavage. These feldspars were colorless, gray, and rarely light yellow, with a vitreous luster and a transparent to translucent appearance. This mineral was the most common gem material in the region and could be found in both bedrock and its regolith.

As reported recently, the augite samples appeared black under daylight-equivalent illumination but dis-

Figure 22. Basalt-hosted gem materials from southeast Vietnam: A subhedral zircon crystal in laterite (A), a garnet xenocryst in basalt (B), and a brown peridot nodule in basalt (C). Photos by Le Ngoc Nang.

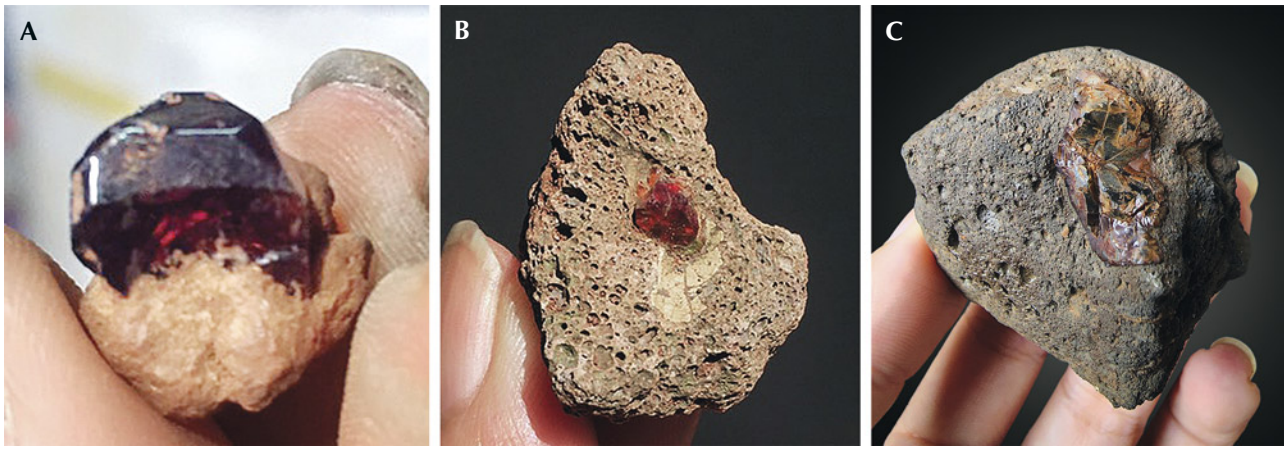

played green and brown colors under transmitted light. Most samples were transparent to translucent and had vitreous luster. The brown gems tended to be more transparent than the green ones (L.N. Nang et al., "Gem-quality augite from Dong Nai, Vietnam," Summer 2023 *G&G*, pp. 182–194).

Brown peridot was found as slightly corroded xenocrystic fragments measuring 0.5–5 cm. The samples were black under reflected light but greenish yellow-brown with transmitted light. Most samples were transparent to translucent, with a vitreous luster. The brown peridot was quite rare and frequently confused with augite due to their similar morphology and occurrence in the vesicular basalt (figure 22C).

The hyalite opal was found in Ba Ria–Vung Tau, and each sample consisted of two parts: the inner body and the outer layer. The contact between the two parts was distinct. The outer layer was opaque white, 2–5 mm thick, and porous. The inner body was usually colorless and rarely green, brown, or light pink, transparent to opaque, with a vitreous appearance. The hyalite opals with good transparency were suitable for jewelry due to their glowing green fluorescence under long-wave ultraviolet light (weak fluorescence under short-wave UV).

Several of these gem deposits in southeast Vietnam are unlicensed. Most materials were collected by locals using artisanal methods, without any commercial mining. The gem materials found along hillslopes or stream channels were extracted at shallow depths ranging from 0.3 to 0.5 m. The gems appeared more frequently after rain and were distributed by their specific gravity. For instance, light material such as hyalite opal was concentrated on the hilltop, stored in slightly weathered and broken-up rock, while heavier minerals, namely sapphire, garnet, feldspar, and peridot, usually accumulated along the hillslopes. Zircon, on the other hand, was often deposited in streambeds. Some gems stored in basalt were extracted easily by homemade tools.

Most of the rough materials are sold to gem dealers in Ho Chi Minh City, who sell fashioned products to local markets in southeast Vietnam. Gemstones in the area have long been gathered by locals during farming and well drilling, but the old-fashioned mining methods led to a significant waste of gem resources. Preliminary evaluations of gem quality have shown that gemstones from southeast Vietnam are of economic potential. The thick basaltic host rock covering a large area is a foundation for prospecting numerous gem materials and requires further research to comprehensively assess available reserves.

Le Ngoc Nang
University of Science, Vietnam National University
Ho Chi Minh City
Liu Gemological Research and Application Center

Pham Minh Tien and Ho Nguyen Tri Man
Liu Gemological Research and Application Center

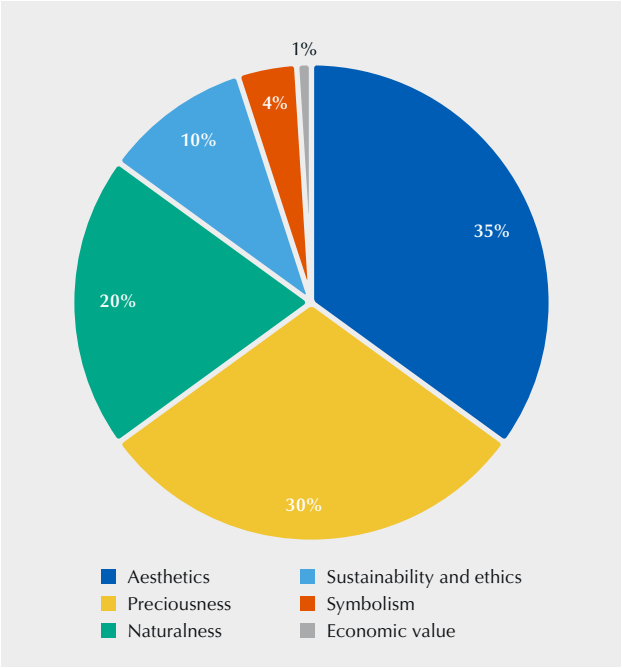

Figure 23. Survey participants identified their top consideration when purchasing colored stones or colored stone jewelry.

Survey of colored stone preferences among younger generations. The global colored stone market is dynamic and constantly evolving. To understand general perceptions and preferences regarding colored stones among designers and potential end consumers from the younger generations, the author conducted a survey in April 2023. The survey targeted 300 respondents under the age of 35, all followers of Donna Jewel (@donna.jewel), an Instagram community designed to champion jewelry from artisans and emerging talents worldwide. Although not scientific, the results of the survey are nonetheless revealing.

Demographics and background: The survey participants consisted of 50% Millennials (born between 1981 and 1996) and 50% from Generation Z (born from 1997 onward). All respondents were over the age of 18. Forty percent were from the United States and another 40% from Europe (specifically Italy, France, the United Kingdom, and Germany), with the remainder split between Latin America (mainly Brazil) and Asia (mainly India and Iran). Respondents identified themselves as gem and jewelry lovers (50%), designers (33%), or gem and jewelry experts (17%).

Colored stone preferences: Participants were asked to choose their single most important consideration when buying colored stones or colored stone jewelry: aesthetics, preciousness, naturalness, sustainability and ethics, symbolism, or economic value. As shown in figure 23, the top two responses were aesthetics (35%) and preciousness (30%). Naturalness was also an important consideration (re-

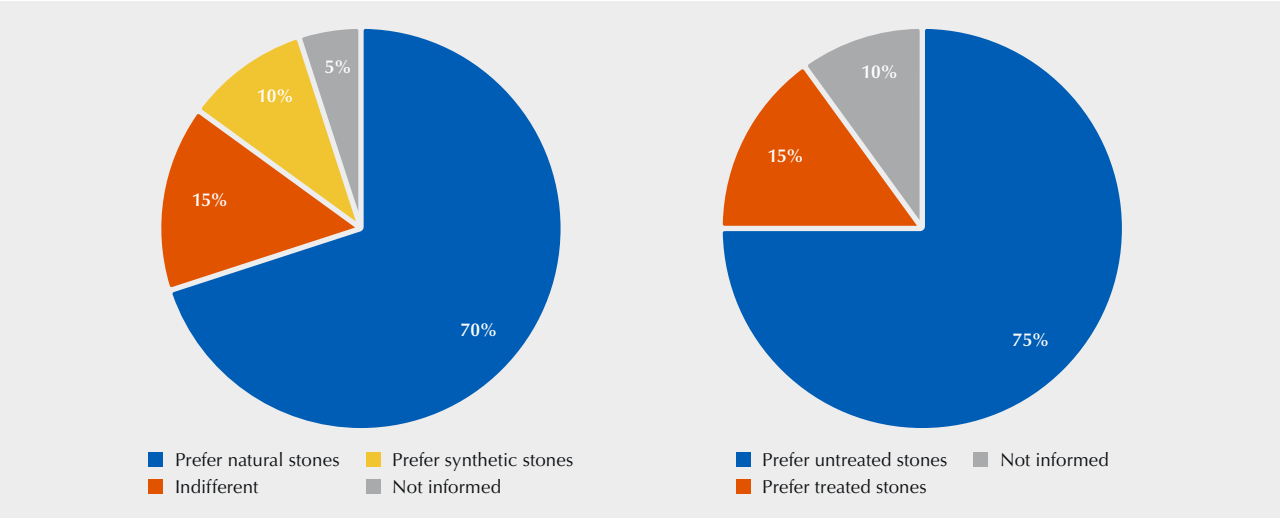

Figure 24. The preferences of survey respondents regarding natural vs. synthetic (lab-grown) gemstones and untreated vs. treated gemstones.

ceiving 20%), while sustainability and ethics was chosen by 10% of the interviewees, symbolism by 4%, and economic value by only 1%.

Given the choice between natural or synthetic gemstones (figure 24, left), 70% chose natural. Only 10% selected synthetic, while an additional 15% expressed no preference. When asked to explain their preferences, the participants who chose natural stones perceived them as unique, rare, and authentic products of nature, capable of evoking emotion, unlike their synthetic counterparts. Those who chose synthetic gemstones viewed them as more sustainable, ethical, and affordable. The topic of natural and synthetic gemstones remains extremely relevant.

Regarding treated vs. untreated natural gemstones (figure 24, right), 75% preferred untreated, which they perceive as more beautiful for their uniqueness and originality. They viewed natural imperfections as an added value lost during treatment. Only 15% preferred treated stones, while 10% acknowledged that they were not informed on the topic.

When asked whether they preferred "precious" or "semi-precious" stones, the participants proved generally indifferent (designers and potential end consumers alike). They associate preciousness with a broader definition more related to uniqueness, emotion, and originality.

Designer perspectives: Designers participating in this survey revealed that they follow both trends and personal inspiration. They noted several uncommon gemstones of particular interest: rainbow obsidian, red beryl, sphene, pargasite, chrysoberyl, scapolite, axinite, enstatite, and benitoite. Fifty percent indicated that they had purchased or used for their jewelry artificially manufactured materials such as glass or cubic zirconia.

At the end of the survey, participants were asked what topics they would be most interested in learning more about. They expressed a strong desire for more knowledge on uncommon and unique gemstones, original colors, treatments, history, lore, origin, and sustainability.

The survey highlighted the younger generations' strong interest in what is unique, original, authentic, and emotional rather than alignment with traditional notions of beauty and preciousness. Naturalness emerged as an important element for the interviewees, who appreciated imperfection as a mark of authenticity and originality. Young designers favored uncommon and original gemstones with distinct and extravagant colors (especially yellows, blues, greens, and reds). While designers sought uniqueness, rarity, and extravagance, potential end customers were also looking for a gemstone with a story to tell.

Laura Inghirami
Donna Jewel, Milan

DIAMOND

Diamondiferous mantle eclogite: Diamond surface features reveal a multistage geologic history. More than 99% of diamonds originally formed in the lithospheric mantle, the cold, rigid mantle that underlies continents, generally <300 km deep (T. Stachel and J.W. Harris, "The origin of cratonic diamonds – Constraints from mineral inclusions," *Ore Geology Reviews*, Vol. 34, No. 1-2, 2008, pp. 5–32). In the lithospheric mantle, the two major rock types—and host rocks for diamond—are peridotite (>95 vol.%), composed predominantly of olivine, and eclogite (<5 vol.%), composed of iron-magnesium-calcium garnet and sodium-rich clinopyroxene. Eclogite is a high-pressure and high-temperature metamorphic rock that can form when dense oceanic crust subducts into the mantle beneath continents at convergent margins.

We cannot directly study the deep portion of the earth where diamonds form. Instead, geologists study diamonds

Figure 25. Mantle eclogite xenolith (2.8 cm in longest dimension) consisting of clinopyroxene (green) and garnet (red-orange), with a partially exposed octahedral diamond. Photo by Annie Haynes. Gift of Mark Mauthner, GIA Museum no. 37511.

themselves, as well as pieces of mantle rock that are transported to the surface as xenoliths by volcanic magmas such as kimberlite or lamproite. The authors have studied one such mantle eclogite xenolith, part of the GIA Museum collection (figure 25). This sample was recovered from a kimberlite in Russia and contained a partially exposed octahedral diamond. The exposed portions of the diamond had visible surface features, including trigons (figure 26).

Trigons are inferred to be etch features that form after diamond crystallization, through interaction with fluids or melts either in the mantle source region or during transport to the surface (J.W. Harris et al., "Morphology of monocrystalline diamond and its inclusions," *Reviews in Mineralogy and Geochemistry*, Vol. 88, No. 1, 2022, pp. 119–166).

Figure 26. Partially exposed diamond embedded in an eclogite xenolith, with positive and negative trigons on the octahedral face. A mineral is included within the diamond, visible through the octahedral face. Photomicrograph by Matthew Hardman; field of view 5.74 mm.

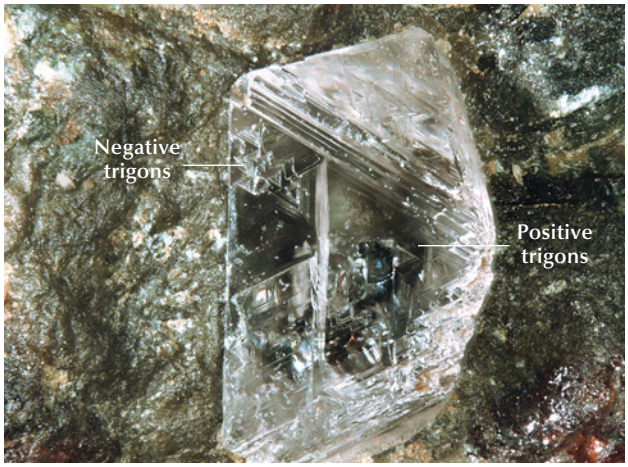

Trigons form exclusively on the octahedral faces of diamond and can have several different orientations. Positive trigons are oriented in the same direction as the octahedral face, and negative trigons have opposing orientation (figure 26). Positive trigons are very rare and may relate to interaction with carbon-oxygen-hydrogen-rich fluids at temperatures between ~800° and 1000°C at near-surface pressures (Z. Li et al., "Positively oriented trigons on diamonds from the Snap Lake kimberlite dike, Canada: Implications for fluids and kimberlite cooling rates," *American Mineralogist*, Vol. 103, No. 10, 2018, pp. 1634–1648). Trigons with negative orientation are much more common. It has been shown experimentally that increasing water content in melts could be one cause for the change of a trigon from positive to negative (e.g., A.F. Khokhryakov and Y.N. Pal'yanov, "The dissolution forms of diamond crystals in $CaCO_3$ melt at 7 GPa," *Russian Geology and Geophysics*, Vol. 41, No. 5, 2000, pp. 682–687). Diamonds with coexisting positive and negative trigons are extremely rare (e.g., Harris et al., 2022) and may indicate that the diamond experienced a complex multistage history related to thermal or fluid changes after its formation.

Using the acquired infrared absorption spectrum, the authors identified the diamond as type IaAB, containing nitrogen in the A- and B-aggregated forms. When the entire xenolith was exposed to ultraviolet light, the diamond fluoresced blue due to N3 defects (three nitrogen atoms surrounding a lattice vacancy), consistent with the presence of nitrogen impurities.

The diamond also contained an unidentified mineral inclusion with visible iridescence (figure 26). Minerals included fully within diamond (which itself is an impermeable time capsule) represent pieces of the mantle source region present at the time of diamond formation. For this sample, the mineral was too deep within the diamond to conclusively identify it nondestructively. However, if the mineral inclusion could be extracted, its chemical composition might be very useful in reconstructing the geologic

Figure 27. Pearl diver collecting shells from the wild. Photo courtesy of Pearls of Australia: Cygnet Bay Pearl Farm, Western Australia.

history of the host diamond, as well as that of the mantle rocks in which the diamond formed.

Matthew F. Hardman and Mei Yan Lai
GIA, Carlsbad

RESPONSIBLE PRACTICES

An environmental, social, and governance assessment of marine pearl farming. Farming pearl oysters is an important economic activity that, when done sustainably, can also provide valuable environmental and social benefits. To gain an evidence-based understanding of the sustainability challenges and opportunities facing marine pearl farming and their intersection with environmental, social, and corporate governance (ESG), The Nature Conservancy (TNC), a U.S.-based nonprofit, conducted an ESG assessment of an Australian pearl farm. This pilot project was intended to guide the development of a sector-wide ESG and sustainability assessment framework. The project was supported and funded by GIA as part of its global effort focused on education and the promotion of responsible practices.

Pearl oysters filter water at rates that are often higher than those reported for other oyster species. This filtration process contributes to waste treatment through the uptake of not only nutrients (nitrogen and phosphorus) but also heavy metals (S. Gifford et al., "Quantification of in situ nutrient and heavy metal remediation by a small pearl oyster (*Pinctada imbricata*) farm at Port Stephens, Australia," *Marine Pollution Bulletin*, Vol. 50, No. 4, pp. 417–422; L.T. Barrett et al., "Sustainable growth of non-fed aquaculture can generate valuable ecosystem benefits," *Ecosystem Services*, Vol. 53, 2022, article no. 101396). Pearl oysters are hung in baskets suspended from long lines, and these structures in which they are farmed provide habitat for a variety of fish and invertebrates (S.J. Theuerkauf et al., "Habitat value of bivalve shellfish and seaweed aquaculture for fish and invertebrates: Pathways, synthesis and next steps," *Reviews in Aquaculture*, Vol. 14, No. 1, 2022, pp. 54–72). If the negative impacts of pearl farming can be mitigated and effective sustainability strategies implemented through waste reduction, recovery and reuse, disease mitigation, and avoidance of overstocking, pearl farming could significantly benefit regional economies and local marine environments.

TNC's 2019 report titled *Towards a Blue Revolution* provided comprehensive guidance for evaluating critical aquaculture systems. Since the report's publication, TNC has built a science-based tool to assess industry and company operations. This tool takes into account factors related to the natural environment as well as the inherent and unique characteristics of a sector or company's operations. The tool has been designed to consider environmental data and the health of local ecosystems, enabling the identification of potential environmental benefits via restorative aquaculture, which has the potential to generate a net positive ecosystem outcome. This approach sets it apart from other sustainability assessment frameworks, risk assessments, and life cycle assessment methodologies.

Between February and May 2023, the assessment was conducted on Cygnet Bay Pearl Farm (CBPF; see figures 27–29), a company that produces pearls from *Pinctada maxima* north of Broome, Western Australia, using both wild capture and hatchery operations. CBPF is an operation of Pearls of Australia (PoA). Using the TNC framework, a number of overarching factors were assessed:

- Company capacity, ethics, and management measures
- Impacts on wild stocks from source of stock, hatchery escapes/interbreeding, and macrofauna interactions
- Reliance on added feed and chemicals
- Habitat impacts
- Water column effects (e.g., temperature, salinity, light penetration, and chemical characteristics of seawater at different depths)
- Disease
- Use of resources: fresh water, land, and energy

Figure 28. The pearl oysters are partially opened to allow seeding. Photo courtesy of Pearls of Australia: Cygnet Bay Pearl Farm, Western Australia.

The assessment showed that CBPF meets or exceeds all essential requirements within the ESG framework, including the company capacity, ethics, and management metrics. The company has no compliance issues associated with sustainability metrics, and an internal management team oversees sustainability topics and implementation. CBPF adheres to the Pearling Environmental Code of Conduct, developed by Australia's Pearl Producers Association in 2002 and updated in 2007. The farm has Marine Stewardship Council certification, meeting independent, third-party ecological sustainability standards. It operates within a country that has an effective governance, legal, and enforcement system in place to manage the industry into the future.

Regarding the social component of ESG, CBPF forms part of the Banararr Steering Committee (BSC) of the Bardi people, the traditional owners of the area. The BSC's role is to establish a positive relationship between CBPF and the Bardi traditional owners. Any amendment, use, or development of the area is discussed by the BSC together with relevant topics affecting the community at large, including school, transport, and fishing. Dedicated cultural heritage tours managed by Bardi people form part of the ecotourism offered at Cygnet Bay Pearl Farm. CBPF is active in research, housing the Kimberley Marine Research Station, and parent company PoA currently partners with the Marine Bioproducts Cooperative Research Centre. This research focuses on better understanding the implications and potential positive effects on fish and invertebrates that grow naturally on PoA farms.

CBPF could already be providing environmental benefits to the surrounding area through restorative aquaculture practices. Based on a general understanding of ecosystem services associated with oyster aquaculture, CBPF does meet the criteria for restorative outcomes, such as increased cycling of water and nutrients and providing habitat to other species. However, the extent to which these ecosystem services positively impact broader environmental outcomes remains unknown, in part because of the limited understanding of anthropogenic effects on water quality and habitat loss in the area.

Overall, the assessment provided an effective means to evaluate CBPF for its management and approach to ESG, the extent to which cultural communities are considered, the company's engagement with voluntary certification and codes of practices, and its awareness of key environmental risks and negative impacts as well as positive impacts.

Figure 29. Seeding Pinctada maxima *pearl shell. Photo courtesy of Pearls of Australia: Cygnet Bay Pearl Farm, Western Australia.*

Figure 30. Akshay Poddar, Melizza and Jennifer Tanpoco, and Julia Hackman Chafé are some of GIA's featured graduates on the Alumni Collective website.

At the same time, additional needs for TNC's ESG Assessment Framework have been identified. Brood stock sourcing and handling, biosecurity, and genetic risks are all areas that require additional research. One hundred percent utilization of the oysters farmed should be an explicit goal and assessment factor. The assessment should also consider the legacy effects of aquaculture equipment (e.g., recovery, reuse, and recycling), as well as the origin and species status of shells utilized to manufacture nuclei. Once these considerations are addressed, the TNC's ESG Assessment Framework should provide an effective sector-wide approach.

Heidi Alleway
The Nature Conservancy
Adelaide, Australia

ANNOUNCEMENTS

GIA Alumni Collective. Discover the GIA Alumni Collective, a networking and knowledge hub for GIA graduates. The online community at collective.gia.edu is a diverse group who all share a passion for the gem and jewelry industry. Users can access both live and self-paced Continuing Education seminars, join virtual chapters, connect with global alumni, and more. The site also highlights some of the GIA alums who uphold GIA's highest standards (figure 30).

Akshay Poddar earned his Graduate Gemologist diploma at GIA's Mumbai campus. A third-generation diamantaire, Poddar was driven to start his own business, dealing in both wholesale trade and retail. The diamond jewelry designer believes that while nature creates the diamond, his job is to add beauty to it.

Jennifer Tanpoco launched Jaune Pearls in 2002, later enlisting her daughter Melizza as CEO. The Tanpocos, both GIA Pearls Graduates, focus on sustainability and long-term environmental impact in their business, educating clients on how the pearls are sourced.

Julia Hackman Chafé used her marketing background and her Colored Stone Essentials Certificate from GIA to create a strong digital presence after taking over social media for her family's wholesale colored stone business. Now a successful influencer under the name JewelsWithJules, Chafé shares photos and videos of gems, jewelry, and international travel, providing her followers with a unique look at the colored stone trade.

Visit https://collective.gia.edu/meet-the-collective.html to read stories from these alumni and more.

Gübelin Gem Museum opens in Switzerland. In July 2023, the Swiss firm Gübelin, known for its luxury timepieces and jewelry and its gemological laboratory, opened the Gübelin Gem Museum in Lucerne, Switzerland (figure 31). The collection allows visitors to explore the formation, origin, and diverse colors of fascinating gemstones (figure 32), as well as the history of the family-owned business, founded in 1854.

The opening of the museum commemorates the 100th anniversary of the Gübelin Gem Lab, which became a world-renowned institution in the field under the leader-

Figure 31. A look inside the new Gübelin Gem Museum in Lucerne, Switzerland. Photo courtesy of Gübelin.

ship of Dr. Edward J. Gübelin. Recognized for his gemstone inclusion research, Dr. Gübelin's groundbreaking work is a focal point of the museum, including many of his instruments and gemstones he collected during his travels worldwide. Visitors will discover 174 gemstones selected from the company's reference collection in addition to selected Gübelin watches and jewelry pieces from various eras.

The compact space not only houses historical exhibits but also provides a window to the future. Visitors will learn about Provenance Proof, the company's blockchain technology for colored gemstones, and Gemtelligence, a colored gemstone analytical tool that uses artificial intelligence to increase consistency in data interpretation, origin determination, and identification of heat treatment. It is also the new home of the Gübelin Academy, offering courses to inspire students in the museum setting. Through digital and interactive elements, the exhibits will be continuously updated and expanded, ensuring new experiences for years to come. For more information, visit www.gubelin-gemmology.com.

Erica Zaidman
GIA, Carlsbad

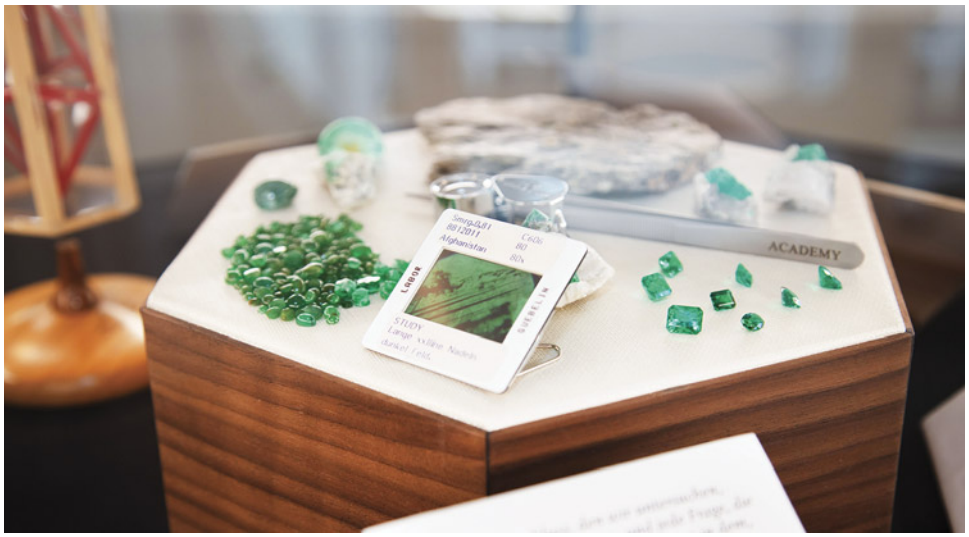

Figure 32. A display case featuring emerald at the Gübelin Gem Museum. Photo courtesy of Gübelin.

CONFERENCE REPORTS

Chicago Responsible Jewelry Conference. The seventh annual Chicago Responsible Jewelry Conference (CRJC) was held August 11–13, 2023, in Rosemont, Illinois. **Susan Wheeler**, Responsible Jewelry Transformative (RJT) founder and Virtu Gem cofounder, opened by highlighting efforts to further the United Nations Sustainable Development Goals (SDGs) and the UN Women's Generation Equality campaign. The first of the 17 SDGs is to end poverty, which disproportionately affects the roughly 40 million artisanal and small-scale miners worldwide. Wheeler said poverty poses a risk to the jewelry industry because consumers do not want to perpetuate it. Responsible supply chains can help lift miners from poverty, she noted, and the industry can make great strides toward the UN's goals.

Anna Samsonova (Samsonova Consulting) moderated a panel on opening markets for artisanal gemstone miners in East Africa. **Pauline Mundia** (Virtu Gem Zambia), **Jessica Hudson** (Virtu Gem), **Sejal Karavadia** (Brilliant Earth), and **Cristina Villegas** (PACT and Moyo Gems) discussed the importance of information exchange with miners and cutters, developing trust with the help of local associations, creating sourcing standards, and training and education. Karavadia said customers are very receptive to a gem's mine-to-market story. Sixty percent of the miners in Moyo's supply chain are women, Villegas said, and they have begun incorporating young woman cutters. "For many years, Africa was exporting raw unprocessed materials," she said. "Now it's high-end beautiful faceted gemstones, and we should celebrate that."

Deep-sea biologist **Lisa Levin** (Scripps Institution of Oceanography, University of California, San Diego) explained how deep-sea mining of minerals, including gold and silver, would disrupt ecosystems. The International Seabed Authority (ISA) has approved 31 mining exploration contracts in international waters as of January 2023 and is developing regulations. Deep-sea ecosystems host abundant life, with interdependent species that depend on specific hydrologic and geochemical properties, she said, and provide many benefits to the broader ocean. The deep sea is also home to bacteria that consume methane, a driver of global warming. Levin said mining could cause extinctions and risks destruction of deep-sea biodiversity. Additionally, scientists believe that post-mining restoration is not possible on the seafloor. Since the definition of serious harm remains unclear and much about these ecosystems is still unknown, she said, there is insufficient knowledge for evidence-based decision making by the ISA.

Holly McHugh (Mejuri, Inc.) moderated a panel on responsible silver sourcing. Panelists noted an increase in high-level guidance for responsible sourcing. Examining this market is complex because more than 70% of silver production is a byproduct of other mining, panelists said, while artisanal and small-scale mining is challenging because silver requires so much mining effort. **Torry Hoover** said Hoover & Strong's refined metals are now 100% recycled, and **Will Nevins-Alderfer's** W.R. Metalarts uses Fairmined silver for its alloys. Many of the Richline Group's larger customers now ask about sourcing, said **Mark Hanna**, and the company has begun tracking silver with blockchain. He emphasized knowing your supplier and customer to ensure ethical products.

Susan Wheeler and Virtu Gem's **Chiko Manda** (via video message) discussed Malawi's gem trade. The country exports hundreds of kilograms of high-quality aquamarine annually but is one of the poorest in the world. Manda said very few gems mined in Malawi are processed there due to lack of expertise and equipment, compounded by smuggling problems, and data indicate that less than 1% of its aquamarine is legally exported. He asked jewelry companies to allocate a small percentage of their budgets to buy cut stones from source countries to motivate cutters to improve their skills. Wheeler added that this would improve traceability. "If you support the gem processing industry in Africa, you empower a lot of people," Manda said.

In a virtual presentation, **Mkhululi Nkosilamandla Ncube** (African Minerals Development Center, AMDC) introduced the African Mining Vision (AMV), a project of the UN. The AMV aims to transform the paradox of mineral wealth and dire poverty through equitable mineral exploitation. The AMDC's methods to implement the AMV include community engagement, training, technology, and financial support. As part of the approach, the Africa Gemstones and Jewellery Exhibition and Conference (AGJEC) series promotes the trade of African gemstones within the continent. The first event was held in Zambia in July; upcoming events will take place in Nigeria and Ghana this fall.

Brecken Branstrator (GemGuide) moderated a panel on working with source country gem traders (figure 33). **Eric Braunwart** (Columbia Gem House), **Ola Erogbogbo-Oyeniyi** (Deinte Designs Limited), Pauline Mundia, **Stuart Pool** (Nineteen48), and Susan Wheeler shared key takeaways, including the importance of understanding the local market and legal system, supply chain analysis, and working with local partners. Erogbogbo-Oyeniyi said that helping a community and weaving that into a gem's story is a great benefit.

Anna Bario described founding jewelry company Bario Neal with fellow designer Page Neal in 2008 and developing a responsible supply chain. Early on, they connected with Ethical Metalsmiths, the Alliance for Responsible Mining (ARM), and artisanal miners in Tanzania and Peru. They built relationships with ethical suppliers over the next decade and in 2019 hired a consultant to help establish a process based on the UN SDGs and OECD Due Diligence Guidance for Responsible Business Conduct. This includes a code of conduct they share with suppliers, supplier interviews, and an eight-step partner and material evaluation process. In 2020, the company released its first biannual sustainability report, possibly the first by a small independent jeweler. Their next goal is Climate Neutral certification.

Figure 33. Pauline Mundia, Susan Wheeler, Eric Braunwart, and Ola Erogbogbo-Oyeniyi discuss working with gem traders in source countries. Photo courtesy of RJT.

A panel on sex trafficking in Marange, Zimbabwe, moderated by **Brandee Dallow** (Grandview Klein Diamond Group), began with a documentary clip of survivors' stories. The area has been fraught with conflict and violence since the discovery of diamonds there in 2006. The U.S. has banned imports of Marange diamonds due to reports of forced labor. According to **Abigail Sibanda** (Marange Women's Alliance, MWA) (figure 34, left), the military, police, mine guards, and informal miners collaborate to smuggle diamonds out and exploit women and girls. Vulnerability to trafficking stems from Zimbabwe's high poverty, and many victims are lured by the promise of mining work. The community questions where the diamond revenue goes because there is no development, Sibanda said. Susan Wheeler noted that RJT and MWA have facilitated support for survivors through court advocacy, but prosecution is still very limited. MWA helps survivors with peer-to-peer counseling and other support and empowers all women to speak out, holding weekly meetings on WhatsApp. The group has been planning to pur-

Figure 34. Left: Abigail Sibanda describes efforts by the Marange Women's Alliance to help women and girls in Zimbabwe. Right: Laura Galvis (ARM) speaks about Fairmined-certified projects combining gold mining and agriculture in Colombia. Photos courtesy of RJT.

chase a chicken coop to develop consistent income and pay for their cellular data, which RJT currently covers. MWA is also creating a billboard campaign for Marange to highlight the issue. "We protect the diamonds. Why don't we protect the women?" remarked Sibanda, who has relocated outside of Zimbabwe because her activism has put her at risk.

Roy Maconachie (University of Bath, England) described the relationship between mining and agriculture in Sierra Leone based on his research there since 2003, after the civil war. Most mining occurs in the dry season, with income used to farm in the rainy season. Over the last decade, artisanal miners have shifted to gold because most alluvial diamond deposits are mined out. Artisanal gold mining here is dominated by women and provides a reliable income. The interconnected nature of farming and mining can help rebuild agricultural institutions destroyed during the war, he said, but miners still need basic infrastructure, access to markets and credit, and technology.

Laura Galvis (ARM) (figure 34, right) detailed three Fairmined-certified projects—the Íquira cooperative, La Gabriela, and the Chede mine—that support almost 200 workers and show how small-scale gold mining and agriculture coexist in Colombia. The Fairmined label certifies gold, silver, and platinum from small-scale mining organizations using responsible practices, and it comes with the Fairmined Premium, an economic incentive. The Chede mine committee will use this year's premium to sponsor a coffee brand sourced by miners farming coffee; they have 5,600 Fairmined credits and need 20,000 for this project. Businesses can buy Fairmined credits to support the project of their choice.

Sarah Yood (Jewelers Vigilance Committee) and **Andrea Hill** (Hill Management Group) discussed U.S. sanctions against Russian diamonds due to the war in Ukraine. Yood explained that because diamonds are considered a product of the country in which they are cut—with 90% cut in India—Russian diamonds can still reach the U.S. She acknowledged India's difficult position and the issue of protecting jobs there. The EU and the G7 countries are working to stop the flow of Russian diamonds. (At press time, an announcement was expected shortly.) Yood said that starting in 2024, G7 countries will likely require diamonds of one carat or larger to carry proof they were not mined in Russia (the size threshold will be progressively lowered). Hill said that in theory, it will eventually be clear if a diamond originated in Russia or Zimbabwe.

Saleem Ali (University of Delaware and UN International Resource Panel, IPA) presented an IPA report analyzing resource rushes in Africa, which found that mineral resources can lead to migration within Africa and prevent migration to Europe. A key message of the report was that property rights to resources can reduce forced migration. Ali suggested jewelry companies partner with the UN High Commission on Refugees to train refugees in jewelry making.

Natasha and Eric Braunwart (Columbia Gem House), **Megan Cochran** (Megan Cochran Jewelry Design), and **Hannah Smythe** (Toast Fine Jewelry) discussed how responsibly sourced designs can engage consumers. The MJSA 2023 Design Challenge, sponsored by Columbia Gem House, asks for designs based on a set of gemstones and a fictional client story. The Jewelry for Wildlife raffle of selected pieces benefits CRRIFS, a wildlife rescue, rehabilitation, and research center in Guaymas, Mexico.

Shannon Kurzyniec and **Chelsea Rowe** of the Ethical Metalsmiths Student Committee introduced 2023's So Fresh + So Clean online responsible jewelry exhibition, which asked artists to consider the life cycle of their creations. This year's awards went to Rashele Alradaideh (Virginia Commonwealth University), Amy Beeler (Bowling Green State University), and Maria Hammond (Manchester Metropolitan University, England), with cash prizes sponsored by Hoover & Strong, Rio Grande, and Earthworks.

The conference also included a collaborative session on advancing the UN SDGs through jewelry supply chains. Sunday offered a Responsible Gem Boutique with eight suppliers, co-located with the InStore Show. After Saturday's sessions, Anna Samsonova announced that attendee donations had fully funded the Marange Women's Alliance's chicken coop project.

Erin Hogarth
GIA, Carlsbad

Turquoise United Conference 2023. The second annual Turquoise United conference was held August 10–12, 2023, at the Albuquerque Convention Center in New Mexico. The vision of the conference is to bring together members of the turquoise industry at a single event for discussion and reunion. With this goal in mind, the conference caters to every aspect of the turquoise industry, attracting miners, lapidaries, collectors, dealers, artists, treatment experts, and researchers. A year ago, GIA representatives attended the inaugural Turquoise United conference (Fall 2022 GNI, pp. 390–394).

This year, there were additional symposium sessions across a range of topics and new competitions for registered conference participants. The first session was hosted by Turquoise Museum executive director **Jacob Lowry**, with a panel consisting of **Kenneth Van Wey** (Indian Arts and Crafts Board), **Matthew Wernz** (Federal Trade Commission), and **Sean Hyrons** (U.S. Fish and Wildlife Service). The panel discussed the laws surrounding the sale and purchase of turquoise jewelry and gave examples of situations in which their respective agencies may become involved (figure 35). The panelists offered advice to consumers purchasing turquoise jewelry, noting the importance of a written receipt stating the authenticity and nature of the product in as much detail as possible.

The turquoise grading system proposed by **Joe Dan Lowry** at last year's conference has been put into practice. Attendees could attempt to grade sample stones or stones

Figure 35. From left: Jacob Lowry, Sean Hyrons, Matthew Wernz, and Kenneth Van Wey engage in a panel discussion titled "Laws: Liabilities and Protections." Photo courtesy of the Turquoise Museum.

of their own using the system based on turquoise master stone sets and grades of color, matrix, and "zat" (boldness and dynamism). Application of the grading system requires detailed knowledge of certain turquoise features present at different mines. For example, author AG did not recognize "waterweb" matrix as being a valuable pattern, and therefore gave a lower matrix score on a stone with a high value. The grading system continues to be developed with feedback from the conference, with a goal of publicly accepted use by 2027.

The conference also offered courses for attendees. A "Turquoise Basics" course taught by Jacob Lowry described the types of turquoise and turquoise imitations in the market to better inform new buyers of the stone. Joe Dan Lowry taught a class called "Collecting 101," offering guidance to consumers beginning their own turquoise collection. A follow-up course, "Collecting 102," is planned for Turquoise United 2024.

Some attendees were rewarded for their impressive specimens and extensive turquoise knowledge. A highest-grade turquoise stone contest received numerous entries from multiple mines, ranging from natural cabochons with striking color and matrix to hefty rough turquoise nuggets. Best in Show winner **Mark Baca** (American Turquoise Online) received a monetary prize and trophy (figure 36). An identification contest over both days of the conference allowed attendees to test their skills at identifying the nature and mine origin of turquoise specimens. **Michael Turano** (Michael Turano Lapidary) won the contest, with **Dye Masaki** (Native Spirit) placing second, and **Ty Gibson** (Gibson Lapidary, LLC) in third.

Author AG presented his research on the Mona Lisa mine, located in western Arkansas, in a session on August 11. He provided details about the history, geology, mineralogy, and current mining operations at the site. Discussion about the methods used and Mona Lisa turquoise's potential place in the market followed the presentation. Material from the mine was also on display at the Turquoise Museum, where the day ended with the Collectors' Circle Gala.

Figure 36. Mark Baca (American Turquoise Online) holds his winning piece (right) and trophy for Best in Show. Photo courtesy of the Turquoise Museum.

Figure 37. Left: A conference participant examines turquoise cabochons. Right: Iranian turquoise cabochon with a brown "spiderweb" matrix pattern. Photos by Aaron Palke.

The following morning, author AP presented GIA's methods for identifying turquoise in the gemological laboratory. Attendees expressed their interest in learning more about these techniques and shared their views on terminology in the turquoise industry.

Next, Joe Dan Lowry presented a session on the challenges of fingerprinting turquoise mine sources, especially in archaeological contexts. The heterogeneity of turquoise, the multitude of sources, and the stone's formation in near-surface, sedimentary environments create unique challenges when trying to determine a stone's mine origin.

Throughout the conference, a gem show focused solely on turquoise was open to the public. Roughly a dozen dealers participated, offering a wide variety of turquoise material (figure 37), including high-end jewelry pieces, natural rough material, untreated cabochons, stabilized cabochons, and beadwork. Many American turquoise localities were represented, while turquoise from Iran, China, Egypt, and Mexico was also available. A silent auction allowed conference attendees to bid on natural turquoise and turquoise jewelry pieces donated by the event sponsors.

The conference concluded with a banquet honoring the first inductees into the Turquoise Hall of Fame: Joseph Pogue, Leonard Hardy, Robert Zachary, Philip Chambless, and James Elquist. These honorees were nominated for their impact on the turquoise industry. The event sponsors reiterated their desire to grow Turquoise United, with confirmation that the annual event will be hosted in Albuquerque in 2024.

Alex Goodsuhm and Aaron Palke
GIA, Carlsbad

ERRATUM

In the Summer 2023 article on augite from Vietnam (pp. 182–194), the carving sizes in figure 1 were incorrectly presented in centimeters. These were the millimeter sizes of the two carvings.